Electronic Spectra of Phenylcyclopropane and Cumene Cation Radicals: Interplay of Experiment and Theory

J. P. Dinnocenzo,*,† M. Merchán,‡ B. O. Roos,§ S. Shaik,¶ and H. Zuilhof||

Department of Chemistry, University of Rochester, Rochester, New York 14627-0216, Departamento de Química Física, Universitat de València, Dr. Moliner 50, Burjassot, E-4100 Valencia, Spain, Department of Theoretical Chemistry, Chemical Centre, P.O. Box 124, S-221 00 Lund, Sweden, Department of Organic Chemistry and the Lise Meitner-Minerva Center for Computional Quantum Chemistry, The Hebrew University, Jerusalem, 91904 Israel, and Laboratory of Organic Chemistry, Department of Biomolecular Sciences, Wageningen Agricultural University, Dreijenplein 8, 6700 HG Wageningen, The Netherlands

Received: April 30, 1998

The structures of phenylcyclopropane ($\mathbf{1}^{+\bullet}$) and cumene ($\mathbf{2}^{+\bullet}$) cation radicals were calculated using both CASSCF and B3LYP computational methods. Both methods predict that $\mathbf{1}^{+\bullet}$ adopts a delocalized, bisected structure and that the barrier to phenyl group rotation is substantial (11−14 kcal/mol). In contrast, the spin and charge in $\mathbf{2}^{+\bullet}$ is largely localized in the phenyl ring and there is no strongly preferred ground state conformation. The CASPT2 method was used to predict the electronic spectra of $\mathbf{1}^{+\bullet}$ and $\mathbf{2}^{+\bullet}$. The large differences in the spectra of $\mathbf{1}^{+\bullet}$ and $\mathbf{2}^{+\bullet}$ can be traced to significant $\sigma-\pi$ interaction in $\mathbf{1}^{+\bullet}$. The results are rationalized in terms of a simple valence bond configuration mixing model. In general, the calculated transition energies were in good accord with the experimental values; however, the relative UV−vis peak intensities for $\mathbf{1}^{+\bullet}$ were not well reproduced if a static structure was assumed. Better agreement was obtained by taking into account libration of the phenyl group in $\mathbf{1}^{+\bullet}$.

I. Introduction

Arylcyclopropane cation radicals have been the subject of increasing interest in recent years.[1] A common conclusion derived from these studies is that the degree of electronic interaction between the aryl and cyclopropyl rings affects the cation radical structures and their reactivities. It was recently pointed out that arylcyclopropane cation radicals can have electronic absorption spectra that differ dramatically from simple alkyl-substituted aromatic cation radicals.[1s] For example, the visible electronic absorption transition of phenylcyclopropane cation radical ($\mathbf{1}^{+\bullet}$) has $\lambda_{max} \approx 540$ nm while that of cumene cation radical ($\mathbf{2}^{+\bullet}$) is ≈440 nm! This large difference contrasts with the corresponding neutral molecules whose longest wavelength UV transitions differ by only 7 nm. In this paper, ground state structures and the electronic spectra of $\mathbf{1}^{+\bullet}$ and $\mathbf{2}^{+\bullet}$ are calculated by state-of-the-art computational quantum chemical methodologies. The results demonstrate a constructive interplay between theory and experiment. On the one hand, the calculations provide insights into the electronic states of $\mathbf{1}^{+\bullet}$ and $\mathbf{2}^{+\bullet}$ that cannot be easily derived from the electronic spectra alone. On the other hand, the spectra provide essential calculational benchmarks. In the case of $\mathbf{1}^{+\bullet}$, they reveal dynamical aspects of the cation radical that would not have been obvious from calculations alone.

Ground state structures were computed with both the hybrid density functional B3LYP method[2] and a multiconfigurational wave function via the CASSCF method.[3] The excited state calculations were performed using the CASSCF method, with dynamical correlation effects computed using second-order perturbation theory (CASPT2).[3] This approach has been successfully used in a number of studies involving $\pi\rightarrow\pi^*$ and $n\rightarrow\pi^*$ excitations in organic molecules, and also for studies of excited states in transition metal complexes.[4,5] The current study is another test case of the method, since it involves a system where $\sigma-\pi$ interaction is important. There is no a priori reason to believe that the method would not work well for such cases and previous results show this to be the case. Calculations at the CASPT2 level on the electronic spectrum of neutral norbornadiene, where both indirect conjugation and $\sigma-\pi$ interaction must be considered, have shown good agreement with experimental data.[5b]

The CASSCF/CASPT2 method has earlier been used to study cation radical spectroscopy with good results.[6] Indeed, cation radicals are cases for which the second-order perturbation treatment of electron correlation is particularly well suited. Since the occupied and virtual spaces are well separated in cation radicals, intruder states in the first-order wave function do not present a problem.

The computational results for $\mathbf{1}^{+\bullet}$ and $\mathbf{2}^{+\bullet}$ are analyzed in terms of a valence bond configuration mixing (VBCM) model[7] that identifies the origins of the different electronic transitions and provides insight into spectral changes associated with dynamic fluctuations in $\mathbf{1}^{+\bullet}$. Previous experience has shown that the combination of CASPT2 calculations and VBCM analysis can provide useful insight into chemcial problems. For example, they have been recently used to understand the underlying factors that determine the regioselectivity of reaction between nonalternant hydrocarbon cation radicals and nucleophiles.[8]

† University of Rochester.
‡ Universitat de València.
§ University of Lund.
¶ Hebrew University.
|| Wageningen Agricultural University.

10.1021/jp9820673 CCC: $15.00
Published on Web 10/13/1998

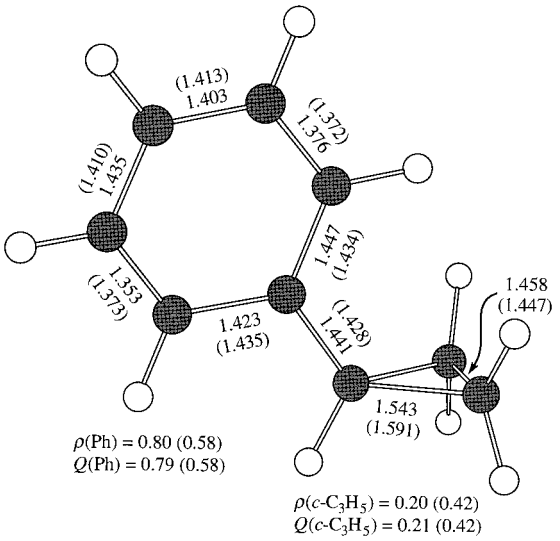

Figure 1. Selected CASSCF/6-31G(d,p) (B3LYP/6-311G(d,p)) bond lengths (angstroms), group spin (ρ), and group charges (Q) for ground state phenylcyclopropane cation radical ($\mathbf{1}^{+\bullet}$).

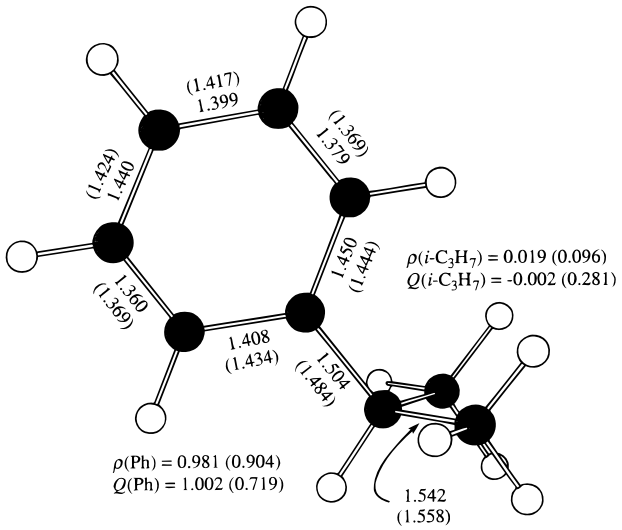

Figure 2. Selected CASSCF/6-31G(d,p) (B3LYP/6-311G(d,p)) bond lengths (angstroms), group spin (ρ), and group charges (Q) for ground state cumene cation radical ($\mathbf{2}^{+\bullet}$) in bisected geometry.

II. Computational Methods

Geometries were optimized at the CASSCF level employing the 6-31G(d,p) basis set. The geometry optimizations were carried out with the GAUSSIAN-94 software.[9] The active space consisted of four orbitals (HOMO-1, HOMO, LUMO, and LUMO+1) with three active electrons for both $\mathbf{1}^{+\bullet}$ and $\mathbf{2}^{+\bullet}$, while four active electrons were used for the neutral systems. The resulting geometric parameters for ground-state $\mathbf{1}^{+\bullet}$ and $\mathbf{2}^{+\bullet}$ are presented in Figures 1 and 2.

Hybrid DFT calculations (B3LYP)[2] and appropriate geometry optimizations were also carried out with the GAUSSIAN-94 series of programs using the 6-311G(d,p) basis set implemented therein. Calculated $\langle S^2 \rangle$ values were ≤ 0.762 in all cases, in good agreement with the theoretically expected value of 0.75 for a pure doublet state. B3LYP results for cation radicals have generally been found to be reliable.[10]

Calculations of the vertical excitation energies were performed at the CASSCF optimized ground state geometries with the CASSCF/CASPT2 method using the MOLCAS-3.1 program system.[11] An ANO type basis set[12] was used with the contractions C[3s2p1d]/H[2s1p], which gives 186 basis functions for the largest molecule $\mathbf{2}^{+\bullet}$. The choice of the active space for $\mathbf{1}^{+\bullet}$ was based on the following arguments. First, we included the six benzene π-orbitals with five active electrons. Second, we included one orbital in each symmetry from the cyclopropyl moiety in order to be able to study the charge-transfer states from the cyclopropyl ring to the phenyl ring. The resulting active space has eight orbitals with nine active electrons. This space should be able to describe the valence $\pi \rightarrow \pi^*$ excitations in the ring and the lowest charge-transfer states. To be consistent, the same active space was used for $\mathbf{2}^{+\bullet}$.

One state-averaged CASSCF calculation was performed in each symmetry for five A″ states of $\mathbf{1}^{+\bullet}$, four A″ states for $\mathbf{2}^{+\bullet}$, and one A′ state for each cation radical. CASPT2 calculations were performed for each of the electronic states. Oscillator strengths were computed from CASSCF transition moments combined with CASPT2 energies, an approach that has been used successfully in a number of earlier applications.[4]

III. Results and Discussion

A. Ground State Cation Radical Structures. Ground state cation radical structures were computed at both CASSCF/6-31G(d,p) and B3LYP/6-311G(d,p) levels of theory. Both methods predict that phenylcyclopropane cation radical adopts a bisected conformation with two equally lengthened C−C bonds (see Figure 1). The results are in agreement with earlier DFT calculations which also indicated a 2L1N (2 longbond, 1 normal bond) structure.[1s]

The 2L1N structure predicted for $\mathbf{1}^{+\bullet}$ is somewhat unusual for cyclopropane cation radicals, which generally prefer 1L2N structures.[13] A search for the 1L2N structure was attempted at the B3LYP/6-311G(d,p) level by incremental rotation around the $C_{Ph}-C_R$ bond. Previous calculations on arylcyclopropane cation radicals have shown that the 1L2N structures prefer a phenyl ring conformation that is twisted relative to the bisected structure.[1s] The twisted conformation maximizes the $\sigma-\pi$ overlap with one of the adjacent cyclopropane σ-bonds and results in its preferential elongation. Rotation about the $C_{Ph}-C_R$ bond in 10° increments leads to a smooth increase in energy with no evidence for a 1L2N minimum. Full geometry optimization was performed at each point, except for the $C_{Ph}-C_R$ twist angle which was fixed. Rotation by 90° leads to the parallel conformation of $\mathbf{1}^{+\bullet}$ which is the transition state for rotational isomerization. This conformation is calculated to be 12.0 kcal/mol higher in energy than the bisected conformation. Similar rotational barriers were obtained with the CASSCF (14.0 kcal/mol) and CASPT2 (10.5 kcal/mol) methods. For comparison, the rotational barrier for neutral **1** is calculated to be only 0.82, 0.12, and 1.3 kcal/mol at the B3LYP, CASSCF, and CASPT2 levels, respectively.

The energy difference between the bisected and parallel conformations of $\mathbf{1}^{+\bullet}$ provides a measure of the stabilizing effect of the cyclopropyl group on the aromatic cation radical. It is interesting to note that this energy difference is similar to the difference between the adiabatic ionization potentials of **1** and **2** ($\approx$8.2 vs 8.73 eV; ΔIP = 12 kcal/mol),[14] which provides an alternative measure of the $\sigma-\pi$ interaction in the ground state of $\mathbf{1}^{+\bullet}$. Finally, we note that the geometry as well as the hindered rotation of $\mathbf{1}^{+\bullet}$ are reminiscent of the cyclopropylcarbinyl cation, where the bisected geometry is preferred over the parallel geometry by a similar amount ($\approx$14 kcal/mol).[15]

The interaction between the phenyl and cyclopropyl moieties in the bisected conformation of $\mathbf{1}^{+\bullet}$ is clearly apparent from

TABLE 1: Calculated Vertical Excitation Energies and Oscillator Strengths for Cumene Cation Radical ($2^{+\bullet}$) and Benzene Cation Radical

state	ΔE_{CASSCF} (eV)	ΔE_{CASPT2} (eV)[a]	f[a]	ΔE_{UV-vis} (eV)[b]
$1^2A''$				
$2^2A''$	0.84	0.70 (0.47)	0.0001 (forbidden)	
$3^2A''$	3.14	2.90 (2.82)	0.0259 (0.0152)	2.8
$4^2A''$	5.21	4.61 (4.83)	0.2071 (0.1362)	4.5
$1^2A'$	3.32	2.62 (2.51)	0.0017 (forbidden)	

[a] ΔE and f for cumene (benzene) cation radical. [b] Spectrum of cumene cation radical.[17]

the group spin and charges in the ground state cation radical (see Figure 1). The CASSCF and B3LYP methods both predict a delocalized structure for $\mathbf{1}^{+\bullet}$, albeit to different degrees. For example, the phenyl group spin and charge densities are greater for the CASSCF method than B3LYP. The consequences of this can also be seen in the two structures, where $r(C_{Ph}-C_R)$ is computed to be longer for CASSCF, consistent with a more phenyl-localized cation radical. For similar reasons, the two equivalent cyclopropyl C−C bond lengths are computed to be shorter at the CASSCF level.

In contrast to $\mathbf{1}^{+\bullet}$, calculations on $\mathbf{2}^{+\bullet}$ did not reveal a strong conformational preference for rotation around the $C_{Ph}-C_R$ bond. At the B3LYP/6-311G(d,p) level of theory, the bisected conformation was favored over the parallel one by 2.2 kcal/mol. Neither of these structures were predicted to be energy minima, however. The lowest energy structure had C_1 symmetry, with one of the C−Me bonds nearly perpendicular to the plane of the phenyl ring. However, this structure was calculated to be only 0.2 kcal/mol lower in energy than the bisected conformation.

The extreme flatness of the potential energy surface for rotation about the $C_{Ph}-C_R$ bond in $\mathbf{2}^{+\bullet}$ is consistent with earlier conclusions derived from ESR studies at low temperature in Freon matrices.[16] It is clear that our calculational results place the various structures too close in energy to confidently assign their relative energies, especially considering the possibility that differential solvation effects may affect their ordering. Consequently, we chose to pursue excited state calculations on the bisected conformation for $\mathbf{2}^{+\bullet}$ because of its similarity to that of $\mathbf{1}^{+\bullet}$. We did not expect the conformation of $\mathbf{2}^{+\bullet}$ to have a significant influence on the electronic transitions. As will be shown, this expectation was supported by subsequent calculations which revealed the observable UV−vis transitions of $\mathbf{2}^{+\bullet}$ to be essentially localized in the phenyl ring. A comparison of the calculated structure for the bisected conformation of $\mathbf{2}^{+\bullet}$ using DFT and CASSCF methods is shown in Figure 2.

B. Cation Radical Electronic Spectra. In the UV−vis region, two absorption maxima have been reported for $\mathbf{2}^{+\bullet}$ in an argon matrix, 2.8 and 4.5 eV.[17] The energies of these maxima are quite similar to those from a variety of other monoalkylbenzene cation radicals obtained in frozen matrices or from gas-phase photodissociation spectra.[18] The calculated electronic transitions for $\mathbf{2}^{+\bullet}$ are in good agreement with experiment (see Table 1). As can be gleaned from the parenthetical values in Table 1, the $\mathbf{2}^{+\bullet}$ excitations closely parallel those of benzene cation radical. The principal configurations of each of the calculated states for $\mathbf{2}^{+\bullet}$, their weights, and group spin and charge densities are given in Table 2. The active orbitals of $\mathbf{2}^{+\bullet}$ are shown in Scheme 1.

All of the excited states are found to be localized in the phenyl ring with the exception of the $1^2A'$ state, which has considerable benzene→isopropyl charge-transfer character. A detailed comparison of the A′ and A″ states will be given in the next section.

SCHEME 1: Active π-Orbitals (a″) and σ-Orbital (a′) for Cumene Cation Radical for the Electronic States $1^2A''-4^2A''$ and $1^2A'$

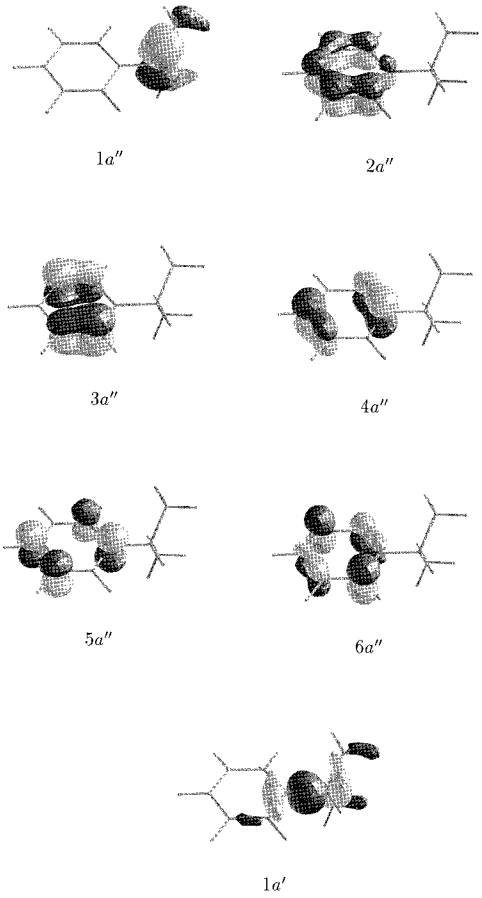

Tables 3 and 4 contain the CASPT2 results for phenylcyclopropane cation radical, as well as experimentally derived transition energies from the UV−vis spectrum of $\mathbf{1}^{+\bullet}$ (Figure 3) and from the photoelectron spectrum (PES) of **1**.[13] As found for $\mathbf{2}^{+\bullet}$, the calculations reveal that the first experimentally observed absorption peak for $\mathbf{1}^{+\bullet}$ is assigned to excitation to the second excited state. The calculations predict three transitions with significant intensity: 2.4, 3.6, and 4.1 eV (unfilled bars in Figure 3). The first and last match up well with the clearly resolved experimental peaks at 2.3 and 4.1 eV. The peak predicted at 3.6 eV is just barely resolved in the experimental spectrum, however. For reasons that will become clear later, the predicted oscillator strength for the 4.0 eV transition is normalized to the experimental peak height in Figure 3. Doing so reveals that the calculated oscillator strength for the 3.6 eV transition is clearly too high relative to experiment, while that for the 2.3 eV transition is marginally low. These discrepancies will be analyzed in detail later when dynamical averaging effects are taken into consideration.

Some comments are warranted here regarding the transition energies derived from the PES spectrum of **1**. The usual practice for extracting electronic transition energies from PES data is to take differences between the *vertical* energy of the first PES band and subsequent ones.[19] This procedure has been most commonly applied in cases of aromatic hydrocarbons where the vertical and adiabatic (onset) IP's are quite similar ($\Delta IP \leq 0.1$ eV). For **1**, however, the ΔIP is ca. 0.5 eV,[14] due to significant structural and electronic reorganization upon ionization. For this reason, we chose to use $\Delta E_{PES} = IP_{n,v} - IP_{0,a}$. This approach provides an estimate of the energy differences between

TABLE 2: Principal Configurations, Weights, Group Charges (Q), and Group Spin Densities (ρ) for Cumene Cation Radical ($2^{+\bullet}$)

state	principal configurations[a]	weight (%)	Q(Ph)	ρ(Ph)	Q(i-C_3H_7)	ρ(i-C_3H_7)
$1^2A''$	$(1a')^2(1a'')^2(2a'')^2(3a'')^2(4a'')^1$	89.4	1.002	0.981	−0.002	0.019
$2^2A''$	$(1a')^2(1a'')^2(2a'')^2(3a'')^1(4a'')^2$	87.5	1.027	0.997	−0.027	0.003
$3^2A''$	$(1a')^2(1a'')^2(2a'')^1(3a'')^2(4a'')^2$	62.7	1.002	0.976	−0.002	0.024
	$(1a')^2(1a'')^2(2a'')^2(3a'')^1(4a'')^1(5a'')^1$	9.8				
$4^2A''$	$(1a')^2(1a'')^2(2a'')^2(3a'')^2(5a'')^1$	63.9	0.966	0.988	0.034	0.012
	$(1a')^2(1a'')^2(2a'')^2(3a'')^1(4a'')^1(6a'')^1$	17.3				
$1^2A'$	$(1a')^1(1a'')^2(2a'')^2(3a'')^2(4a'')^2$	87.5	0.628	0.458	0.372	0.542

[a] The active orbitals are shown in Scheme 1.

TABLE 3: Calculated Vertical Excitation Energies and Oscillator Strengths for Phenylcyclopropane Cation Radical ($1^{+\bullet}$)

state	ΔE_{CASSCF} (eV)	ΔE_{CASPT2} (eV)[a]	f	ΔE_{UV-vis} (eV)[a]	ΔE_{PES} (eV)[b]
$1^2A''$					
$2^2A''$	1.35	1.15	0.0005		1.0
$3^2A''$	2.97	2.40	0.1147	2.3	2.4
$4^2A''$	4.27	3.63	0.1313	3.6	3.5
$5^2A''$	4.85	4.14	0.3076	4.1	4.0
$1^2A'$	3.02	2.97	0.0044		2.8

[a] See Figure 3. [b] Taken from ref 14.

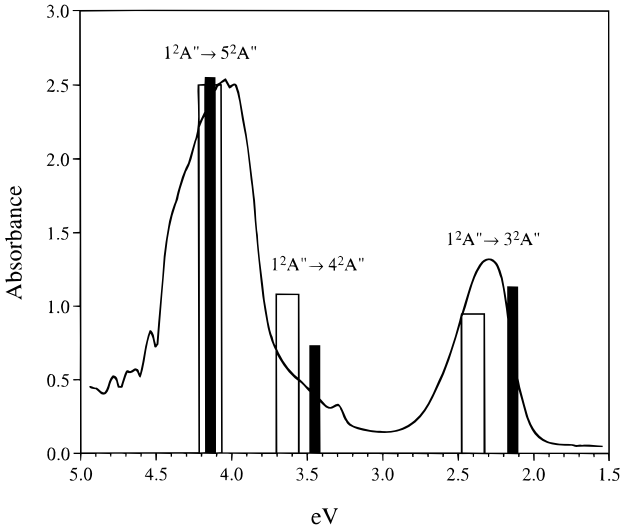

Figure 3. UV−vis spectrum of $\mathbf{1}^{+\bullet}$ in a Freon matrix at 77 K with calculated transition energies and relative oscillator strengths. The unfilled vs filled bars refer to calculated transition energies at a bisected geometry vs one where the phenyl−cyclopropyl twist angle is 30° (see text).

the relaxed cation radical and the vertical cation radical, albeit in the neutral geometry. Admittedly, this latter caveat makes the comparison less than ideal. Despite this limitation, the agreement with the calculated data is surprisingly good (see Table 3). We should point out, however, that, in the case of the $5^2A''$ state, the agreement is somewhat surprising because our calculations show that this state corresponds to an excitation to a virtual orbital. One interpretation of the results is that PES ionization results in conversion to a non-Koopman's state.[19,20]

The active orbitals for $\mathbf{1}^{+\bullet}$ are drawn in Scheme 2, and the dominant CASSCF configurations of the various states are listed in Table 4. As seen from Table 4, all of the excited states for $\mathbf{1}^{+\bullet}$ have a single dominant electronic configuration, although there is a general trend toward more mixed character as the energies of the states increase. The group spin and charges show that the excited states have different extents of charge-transfer character. Some states have mixed character (e.g., $3^2A''$ and $4^2A''$) like the ground state, while others are largely localized on either the phenyl or cyclopropyl rings ($2^2A''$, $1^2A'$, and $5^2A''$). The makeup of these states will be analyzed in detail by the valence bond configuration mixing model described in the next section, and a link will be drawn between the spectra and the structural features of the cation radicals.

It is instructive at this point to comment on the trends in the oscillator strengths in Tables 1 and 3. The transition moment M_{ij} is given by the corresponding electric dipole (μ) matrix element between the ground state $\Phi_0(1^2A'')$ and the excited state Φ_i. If we restrict attention to the dominant single determinants in Tables 2 and 4, the matrix elements between the states is reduced to a matrix element between the active orbitals that participate in the excitation. Thus if the excited state involves excitation from orbital $\langle a|$ to $|r\rangle$, the transition moment will simply be given by $\langle a|\mu|r\rangle$. The larger the "overlap" of the orbitals, the larger the transition moment will be. This qualitative reasoning can be applied to $\mathbf{1}^{+\bullet}$ by appeal to Table 4 and Scheme 2. The $2^2A''$ state arises from the ground state by the 3a″→4a″ orbital excitations. Orbital 3a″ (Scheme 2) is a pure benzene orbital with a node at the attachment sites, while 4a″ is a delocalized orbital with large coefficients at the attachment sites. The dissimilarity of the orbitals results in a low oscillator strength and, consequently, the first excited state will not be easily detected. The $3^2A''$, $4^2A''$, and $5^2A''$ states arise from $1^2A''$ by the orbital excitations 2a″→4a″, 1a″→4a″,

TABLE 4: Principal Configurations, Weights, Group Charges (Q), and Group Spin Densities (ρ) for Phenylcyclopropane Cation Radical ($1^{+\bullet}$)

state	principal configurations[a]	weight (%)	Q(Ph)	ρ(Ph)	Q(i-C_3H_7)	ρ(i-C_3H_7)
$1^2A''$	$(1a')^2(1a'')^2(2a'')^2(3a'')^2(4a'')^1$	88.3	0.79	0.797	0.21	0.203
$2^2A''$	$(1a')^2(1a'')^2(2a'')^2(3a'')^1(4a'')^2$	85.9	0.96	1.010	0.04	−0.010
$3^2A''$	$(1a')^2(1a'')^2(2a'')^1(3a'')^2(4a'')^2$	67.8	0.58	0.784	0.42	0.216
	$(1a')^2(1a'')^2(2a'')^2(3a'')^2(5a'')^1$	7.0				
$4^2A''$	$(1a')^2(1a'')^1(2a'')^2(3a'')^2(4a'')^2$	53.5	0.61	0.514	0.39	0.486
	$(1a')^2(1a'')^2(2a'')^1(3a'')^2(4a'')^2$	12.0				
	$(1a')^2(1a'')^2(2a'')^2(3a'')^2(5a'')^1$	6.1				
$5^2A''$	$(1a')^2(1a'')^2(2a'')^2(3a'')^2(5a'')^1$	57.0	0.67	0.983	0.33	0.017
	$(1a')^2(1a'')^2(2a'')^2(3a'')^2(6a'')^1$	16.1				
$1^2A'$	$(1a')^1(1a'')^2(2a'')^2(3a'')^2(4a'')^2$	87.9	0.24	0.027	0.76	0.973

[a] The active orbitals are shown in Scheme 2.

SCHEME 2: Active π-Orbitals (a″) and σ-Orbital (a′) for Phenylcyclopropane Cation Radical for the Electronic States $1^2A''-5^2A''$ and $1^2A'$

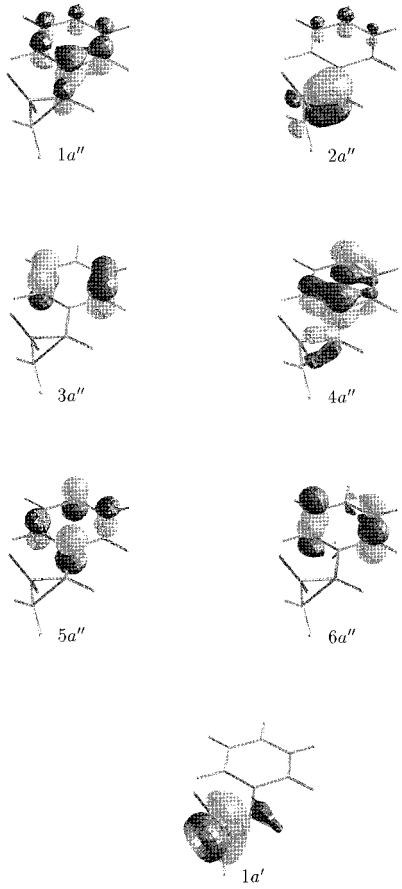

and 4a″→5a″, respectively. These orbital pairs have more similarity and thus lead to higher oscillator strengths for their respective transitions. Finally, the $1^2A''\rightarrow 2^2A'$ transition involves charge transfer from the cyclopropyl-centered 1a′ orbital to the delocalized and phenyl-centered 4a″ orbital. As expected, this results in a low oscillator strength. Analogous arguments can be applied to understanding the relative oscillator strengths for the excitations of $\mathbf{2}^{+\bullet}$.

C. Valence Bond Configuration Mixing Model. In order to conceptualize the spectra and their relation to the structural features of the cation radicals, we will reconstruct the ground and excited states from building block VB configurations.[7] The VB configurations arise by distributing the "active" electrons in orbitals of the constituent fragments of the cation radicals. Subsequently, the configurations will be mixed to yield states. Since we are principally interested in qualitative insight, the VB configuration basis set is kept to the minimum required to provide a lucid picture, and yet one that captures the essential qualitative features.

Figure 4 depicts the VB configurations for $\mathbf{1}^{+\bullet}$. The fragments are benzene (**B**) and cyclopropane (**C**). The first configuration shown depicts the fragment orbitals that are required for interpretation of the spectra. Benzene is represented by four π-orbitals and one σ-orbital. Three of the four π-orbitals of benzene are those that are occupied in neutral **1**; the fourth orbital is one of the degenerate virtual π-orbitals. Cyclopropane is represented by two Walsh orbitals. All of the other fragment orbitals are not shown.

The local symmetry of the π-orbitals is classified according to the mirror plane (m) bisecting the cyclopropane ring, as well

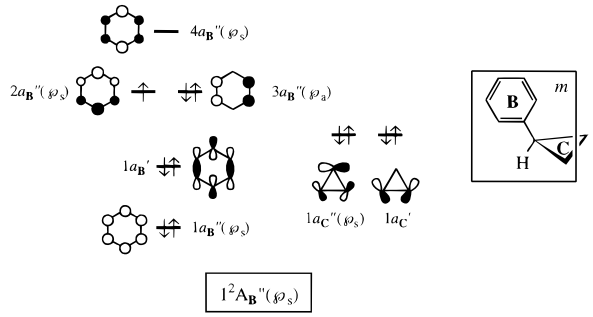

Fragment Hole-State	**B**-Orbitals					**C**-Orbitals	
	$1a_B''(\wp_s)$	$1a_B'$	$2a_B''(\wp_s)$	$3a_B''(\wp_a)$	$4a_B''(\wp_s)$	$1a_C''(\wp_s)$	$1a_C'$
$1^2A_B''(\wp_s)$	2	2	1	2	0	2	2
$2^2A_B''(\wp_a)$	2	2	2	1	0	2	2
$3^2A_B''(\wp_s)$	1	2	2	2	0	2	2
$4^2A_B''(\wp_s)$	2	2	0	2	1	2	2
$1^2A_B'$	2	1	2	2	0	2	2
$1^2A_C''(\wp_s)$	2	2	2	2	0	1	2
$1^2A_C'$	2	2	2	2	0	2	1

Figure 4. Fragment Configurations for $\mathbf{1}^{+\bullet}$.

as the pseudosymmetry (p) with respect to the attachment sites of the fragments. Thus a fragment orbital with a node at the site of attachment is labeled pseudoantisymmetric (p_a), while an orbital with a coefficient at this site is labeled pseudosymmetric (p_s). For example, the orbital labeled $1a_B''(p_s)$ is a benzene orbital (**B**) that is antisymmetric to the mirror plane (therefore a″) and pseudosymmetric (p_s) with respect to the attachment.

The assignment of the fragment configuration symmetry follows from the orbital symmetry. Thus the first configuration is labeled as $1^2A_B''(p_s)$, which means that it is the lowest benzene-localized configuration of A″ symmetry and is pseudosymmetric. The second configuration $2^2A_B''(p_a)$ has the odd electron in the benzene orbital $3a_B''(p_a)$. This configuration lies above $1^2A_B''(p_s)$ due to the Jahn−Teller distortion, which is apparent in the benzene moiety of the cation radical. The configuration $3^2A_B''(p_s)$ places the odd electron in the lowest energy π-orbital and is therefore higher in energy than both $1^2A''$ and $2^2A''$. Still higher in energy is $4^2A_B''(p_s)$, which has the odd electron in the originally virtual orbital $4a_B''(p_s)$. The fifth benzene configuration is $1^2A_B'$, where the odd-electron is localized in the $1a_B'$ σ-orbital of benzene. There are also two cyclopropyl-localized configurations $1^2A_C''(p_s)$ and $1^2A_C'$ where the odd electron is distributed in the two Walsh orbitals, $1a_C''(p_s)$ and $1a_C'$.

Figure 5 shows the configurations for cumene cation radical ($\mathbf{2}^{+\bullet}$). The benzene-localized configurations are the same as for $\mathbf{1}^{+\bullet}$, i.e., n^2A_B'' ($n = 1-4$) and $1^2A_B'$. The isopropyl-localized configurations are nascent from the three high-lying orbitals labeled $1a_P'$, $2a_P'$, and $1a_P''(p_s)$. Distribution of electrons in these orbitals gives rise to $1^2A_P'$, $2^2A_P'$, and $1^2A_P''(p_s)$.

We now turn to the VB interaction diagram in Figure 6 which shows the VB mixing of the configurations to yield the final states of the cation radicals. In the middle of the diagram the benzene-localized configurations are ordered by their relative energies. The hole-localized $1^2A_B''(p_s)$ and $2^2A_B''(p_a)$ configurations are separated by 0.5 eV, which corresponds to the vertical Jahn−Teller splitting taken directly from the CASPT2 calculation on benzene cation radical (Table 1). The rest of the benzene-localized configurations are arranged from photoelec-

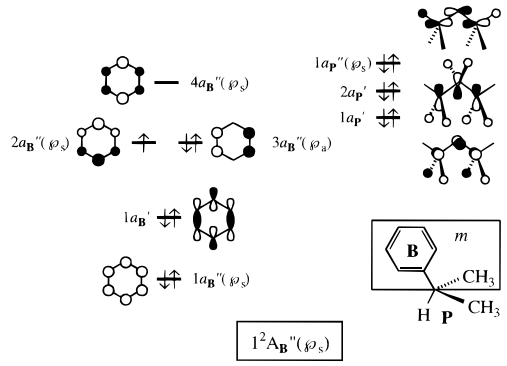

Fragment Hole-State	**B**-Orbitals					**P**-Orbitals		
	$1a_B''(p_s)$	$1a_B'$	$2a_B''(p_s)$	$3a_B''(p_a)$	$4a_B''(p_s)$	$1a_P'$	$2a_P'$	$1a_P''(p_s)$
$1^2A_B''(p_s)$	2	2	1	2	0	2	2	2
$2^2A_B''(p_a)$	2	2	2	1	0	2	2	2
$3^2A_B''(p_s)$	1	2	2	2	0	2	2	2
$4^2A_B''(p_s)$	2	2	0	2	1	2	2	2
$1^2A_B'$	2	1	2	2	0	2	2	2
$1^2A_P'$	2	2	2	2	0	1	2	2
$2^2A_P'$	2	2	2	2	0	2	1	2
$1^2A_P''(p_s)$	2	2	2	2	0	2	2	1

Figure 5. Fragment Configurations for $\mathbf{2}^{+\bullet}$.

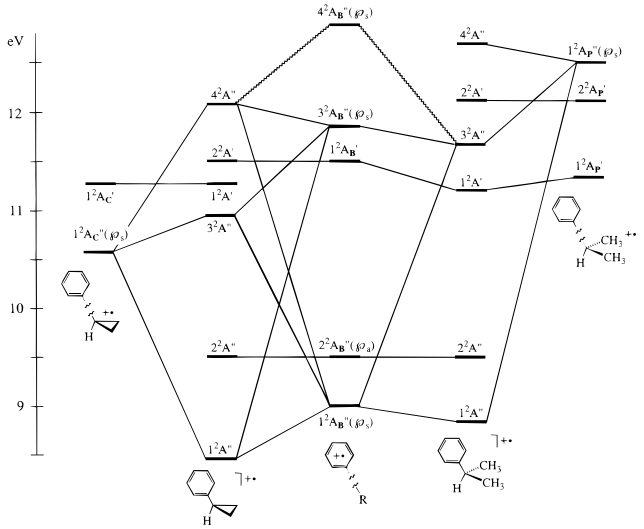

Figure 6. VBCM Diagram for states of $\mathbf{1}^{+\bullet}$ and $\mathbf{2}^{+\bullet}$. R = *i*-C_3H_7 or *c*-C_3H_5 for the benzene-localized fragment states shown in the middle.

tron spectroscopy data.[21] The left-hand side of the diagram contains the cyclopropyl-localized configurations, which are split due to Jahn−Teller distortion. As can be seen from the mixing diagram, the energetic proximity of the cyclopropyl−localized configurations to the benzene−localized configurations will result in a strong interaction that delocalizes the cation radical state into the cyclopropyl moiety thereby causing the Jahn−Teller splitting of its configurations. The right-hand side of Figure 6 contains the isopropyl-localized configurations, which are seen to be high-lying and well separated from the benzene-localized ground configuration $1^2A_B''(p_s)$. This large energy gap will necessarily lead to a weak mixing between the fragment hole configurations and results in a principal difference between $\mathbf{1}^{+\bullet}$ and $\mathbf{2}^{+\bullet}$.

We now focus on the detailed VB mixing interactions. Firstly, the benzene hole configuration $2^2A_B''(p_a)$ does not find a pseudosymmetry match with the cyclopropyl-localized configurations and thus remains a benzene-localized $2^2A''$ hole-state. The three hole configurations with p_s symmetry will mix to form the three states $1^2A''$, $3^2A''$, and $4^2A''$ of $\mathbf{1}^{+\bullet}$. The $1^2A''$ state is nascent from the benzene-localized hole configuration $1^2A_B''(p_s)$ which mixes with $1^2A_C''(p_s)$ in a bonding fashion. The mixing of $3^2A_B''(p_s)$ into $1^2A_B''(p_s)$ is *indirect* and is induced via $1^2A_C''(p_s)$, which mixes with both benzene configurations. This intermixing of the benzene-localized hole-configurations via the cyclopropyl configuration is a polarization effect,[22] which acts to increase the bonding interaction of $1^2A_B''(p_s)$ with $1^2A_C''(p_s)$. The imprints of this polarization are seen in the active CASSCF orbitals 1a″ and 4a″ in Scheme 2, which show that the benzene coefficients at the attachment site increase at the expense of the remote sites. All in all, the VB mixing stabilizes the $1^2A_B''(p_s)$ configuration by 0.65 eV, which together with the Jahn−Teller splitting accounts for the first calculated transition energy at 1.15 eV (Table 3).

The $3^2A''$ state of $\mathbf{1}^{+\bullet}$ arises from the opposing $1^2A_C''(p_s)-3^2A_B''(p_s)$ bonding interactions and the $1^2A_C''(p_s)-1^2A_B''(p_s)$ antibonding interactions. As such, the $3^2A''$ state rises only slightly (0.2 eV) above the $1^2A_C''(p_s)$ localized configuration from which it is derived. Thus the $1^2A''\rightarrow 3^2A''$ transition has a low energy onset at 2.4 eV that is composed of the energy gap of the configurations (1.6 eV), the stabilization of the ground state (0.65 eV), and the destabilization of $3^2A''$ (0.15 eV). The highly mixed character of $3^2A''$ is apparent from the spin and charge densities in Table 4, while its essentially nonbonding nature is apparent from the 2a″ orbital (Scheme 2), which has a node at the attachment sites.

The third A″ excited state, $4^2A''$, arises from the antibonding combination of $3^2A_B''(p_s)$ and $1^2A_C''(p_s)$, with some contribution of $1^2A_B''(p_s)$. However, this state does not rise significantly in energy because of the polarization effect due to mixing with $4^2A_B''(p_s)$, which reduces the antibonding interaction. As such, the $4^2A''$ state remains only 3.62 eV above the ground state. The mixed character of this state is again apparent from the charge and spin densities in Table 4. The uppermost A″ state, $5^2A''$, is nascent from $4^2A_B''(p_s)$ which is lowered by polarization due to mixing of higher lying hole configurations and is not shown in the diagram. The dominant benzenic character of this state is apparent from Table 4.

The last feature regarding $\mathbf{1}^{+\bullet}$ is the localization of the A′ states. The diagram shows two states: $1^2A'$ and $2^2A'$. The $1^2A'$ state is nascent from the cyclopropyl-localized hole configuration $1^2A_C'$. This configuration does not mix with the benzene-localized $1^2A_B'$ configuration due to the virtually zero coefficient of the cyclopropyl Walsh orbital ($1a_C'$ in Figure 4) at the site of attachment. As such, $1^2A'$ is a benzene→cyclopropyl charge-transfer state, which can be seen from the group spin and charges in Table 4. As shown in Figure 6, the energy difference between the $1^2A'$ and ground states is the sum of the initial configuration energy gap (2.3 eV) plus the stabilization of the ground state by VB mixing (0.65 eV). The second state, $2^2A'$, is a pure benzene-hole state nascent from the $1^2A_B'$ configuration. This state is expected to have an extremely low oscillator strength and was therefore not calculated.

We now turn to the VB mixing diagram for cumene cation radical ($\mathbf{2}^{+\bullet}$) shown on the right-hand side of Figure 6. It is apparent that, as opposed to $\mathbf{1}^{+\bullet}$, the $^2A''(p_s)$ hole configurations are separated by significant energy gaps which, taken together with the unfavorable coefficient of the $a_P''(p_s)$ orbital of the isopropyl moiety, will result in a weak VB interaction. Indeed, the stabilization energy of the ground state $1^2A''$ is only ≈0.2 eV. This is the origin of the very low excitation energy of the

first electronic transition at 0.7 eV. We recall that the same band in $\mathbf{1}^{+\bullet}$ appears at 1.15 eV as a result of significant stabilization of the ground state.

Another interesting feature in $\mathbf{2}^{+\bullet}$ is the appearance of the $1^2A'$ state at 2.62 eV above the ground state. This $1^2A'$ state is different than the corresponding $1^2A'$ state in $\mathbf{1}^{+\bullet}$. The origin of the difference is that the $1a_{\mathbf{P}}'$ orbital is the out-of-plane pseudo-π-orbital of the isopropyl group and can therefore mix with the corresponding $1a_{\mathbf{B}}'$ orbital, as shown below. Since the $1^2A_{\mathbf{P}}'$ and $1^2A_{\mathbf{B}}'$ configurations differ by a single electron shift between the two a′ orbitals, the VB mixing will be proportional to the overlap of the orbitals. Thus the $1^2A'$ state of $\mathbf{2}^{+\bullet}$ has a highly mixed benzene−isopropyl character, which is apparent from Table 2.

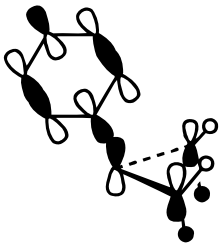

The $2^2A_{\mathbf{P}}'$ configuration is analogous to $1^2A_{\mathbf{C}}'$ discussed above. Due to the pseudosymmetry mismatch, $2^2A_{\mathbf{P}}'$ does not mix well with the benzene hole-configurations and will generate the localized $2^2A'$ state. The transition to this A′ state from the $1^2A''$ ground state is expected to have a very low oscillator strength and was therefore not calculated. Finally, the $3^2A''$ state of $\mathbf{2}^{+\bullet}$ is nascent from the $3^2A_{\mathbf{B}}''(p_s)$ configuration which is stabilized by polarization with $4^2A_{\mathbf{B}}''(p_s)$ and due to a bonding interaction with $1^2A_{\mathbf{P}}''(p_s)$.

Spectra of $\mathbf{1}^{+\bullet}$ and $\mathbf{2}^{+\bullet}$ as Probes of Structure. As described above, the differences in the spectra of $\mathbf{1}^{+\bullet}$ and $\mathbf{2}^{+\bullet}$ reflect the differences in the mixing of the localized hole-configurations and, as such, are characteristic of the structures of the ground state cation radicals. In $\mathbf{1}^{+\bullet}$, the lowest transition energy (1.15 eV) is shifted to the blue by 0.45 eV relative to $\mathbf{2}^{+\bullet}$. This difference is due to the better VB mixing of the benzene-localized configuration $1^2A_{\mathbf{B}}''(p_s)$ with the cyclopropyl-localized configuration $1^2A_{\mathbf{C}}''(p_s)$. The same factor is responsible for the structure of the cation radical. Thus, as can be seen from Figure 1, the structure of $\mathbf{1}^{+\bullet}$ shows that the benzene and cyclopropyl moieties are both distorted as expected from Jahn−Teller distortions. The phenyl moiety adopts a quinoid structure with two short and four long bonds, while the cyclopropyl moiety adopts a structure with two long and one short C−C bonds. Since the parent cyclopropane cation radical undergoes the counterpart Jahn−Teller distortion to a 1L2N structure, the structure of $\mathbf{1}^{+\bullet}$ is clearly nascent from mixing with the hole configuration of benzene. In addition, the C−C bond connecting the two groups undergoes shortening. These structural features cause Jahn−Teller splitting of the localized hole configurations of the two moieties and, in turn, this is manifested in the location of the 2.4 and 2.97 eV excitation energies. Moreover, we recall that the root cause of the blue-shifted, first transition in $\mathbf{1}^{+\bullet}$ is the larger stabilization energy of the $1^2A''$ state of $\mathbf{1}^{+\bullet}$ relative to $\mathbf{2}^{+\bullet}$. This stabilization energy also appears in the rotational barriers of $\mathbf{1}^{+\bullet}$ (≈12 kcal/mol) vs $\mathbf{2}^{+\bullet}$ (≈2 kcal/mol). Therefore, it follows that the spectra of $\mathbf{1}^{+\bullet}$ and $\mathbf{2}^{+\bullet}$ contain fingerprints of the relative cation radical structures.

In this respect, it is interesting to discuss the recently reported effect of phenyl-ring substituents on the 2.4 eV transition of $\mathbf{1}^{+\bullet}$.[1s] Donor substituents were found to cause a blue shift of the absorption maximum while acceptor substituents caused a red shift. As described above, the 2.4 eV peak in the parent cation radical is assigned to the $1^2A''\rightarrow 3^2A''$ transition. This transition corresponds to excitation between two states that are linked by the VB mixing in Figure 6. It should be clear that a donor substituent will stabilize the $1^2A_{\mathbf{B}}''(p_s)$ hole configuration. Consequently, the $1^2A_{\mathbf{B}}''(p_s)-1^2A_{\mathbf{C}}''(p_s)$ configuration gap will increase and the VB mixing will decrease. This will tend to localize the cation radical more on the benzene moiety and consequently the Jahn−Teller splitting will be transferred less to the cyclopropyl moiety. This results in an energy increase in the initial $1^2A_{\mathbf{C}}''(p_s)$ hole configuration by 0.3−0.4 eV. Taken together, these effects will result in a blue shift of the $1^2A''\rightarrow 3^2A''$ transition. Obviously, an acceptor substituent will have an opposing effect, raising $1^2A_{\mathbf{B}}''(p_s)$, thereby enhancing the VB mixing and transferring more of the Jahn−Teller splitting to the cyclopropyl group, which responds by lowering the $1^2A_{\mathbf{C}}''(p_s)$ hole configuration. These effects will contribute to a red shift in the $1^2A''\rightarrow 3^2A''$ transition. Finally, the above analysis leads to the straightforward prediction that the phenyl-group rotational barrier will be affected by substituents on the aromatic ring. The energy should decrease for donor substituents and increase for acceptor substituents.

Effect of Phenyl Group Rotation on the Spectrum of $\mathbf{1}^{+\bullet}$. The energy surface for rotation about the cyclopropyl-phenyl C−C bond in $\mathbf{1}^{+\bullet}$ is calculated to be relatively flat for modest distortions. At the B3LYP/6-311G(d,p) level of theory, rotation by 30° leads to a structure that is only 1 kcal/mol higher in energy than the minimum energy bisected cation radical (**3a**→**3b**). It is expected, therefore, that the experimental spectrum of $\mathbf{1}^{+\bullet}$ might well be rotationally averaged over this distortion. In **3b**, the phenyl ring approximately eclipses one of the cyclopropyl C−C bonds. This results in $\sigma-\pi$ overlap between the C_1-C_2 σ-bond and the phenyl π-system, causing the cyclopropyl group to undergo a structural fluctuation from a 2L1N to a 1L2N structure. Since C_s symmetry is lost during this process, it is expected that the spectra might be altered by rotational averaging, especially the oscillator strengths. Therefore, it seemed important to calculate the effect of phenyl rotation on the electronic spectrum of $\mathbf{1}^{+\bullet}$.

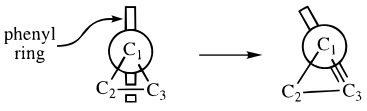

3a **3b**

Before discussing the calculational results, we will first analyze the problem from a VBCM point of view by appeal to Figure 6. Upon phenyl rotation, the symmetry reduction to C_1 will cause the $1^2A'$ state of $\mathbf{1}^{+\bullet}$ to mix with the n^2A'' states, but especially with $3^2A''$ and $4^2A''$, which are closest in energy. $3^2A''$ has nonbonding character resulting from the mixing of $1^2A_{\mathbf{C}}''(p_s)$ with $1^2A_{\mathbf{B}}''(p_s)$ and $3^2A_{\mathbf{B}}''(p_s)$ in bonding and antibonding fashions, respectively. Consequently, the mixing of $1^2A'$ with $3^2A''$ will tend to be small and the electronic essence of $3^2A''$ will be essentially preserved. In contrast, the $4^2A''$ state has a dominant $3^2A_{\mathbf{B}}''(p_s)$ character that will allow strong mixing with the $1^2A'$ state. These trends can also be deduced from inspection of the active orbitals in Scheme 2. Recall that the $1^2A'$ and $3^2A''$ states differ by the occupation of the 1a′ and 2a″ orbitals, respectively. Since the latter has a node on the benzene carbon at the attachment site, mixing of $3^2A''$ with $1^2A'$ will be small. In contrast, the $1^2A'-4^2A''$ mixing results

TABLE 5: CASPT2 Calculated Vertical Excitation Energies (ΔE, eV) and Oscillator Strengths (f) for Phenylcyclopropane Cation Radical ($1^{+\bullet}$) upon Phenyl Group Rotation

state[a]	0°, ΔE (f)	20°, ΔE (f)[b]	30°, ΔE (f)[b]
$2^2A''$	1.15 (0.0005)	1.12 (0.0006)	1.08 (0.0005)
$3^2A''$	2.40 (0.1147)	2.25 (0.1361)	2.14 (0.1372)
$4^2A''$	3.63 (0.1313)	3.55 (0.0966)	3.45 (0.0890)
$5^2A''$	4.14 (0.3076)	4.13 (0.3258)	4.14 (0.3084)
$1^2A'$	2.97 (0.0044)	2.64 (0.0034)	2.67 (0.0019)

[a] State symmetries in bisected geometry (0°). [b] Except for the $C_{Ph}-C_R$ twist angle, calculations were performed using the geometry of the bisected cation radical.

from the $1a'-1a''$ orbital mixing, which will be significant since $1a''$ has a large coefficient on the benzene site of attachment. Since the $4^2A''$ state acquires significant $1^2A'$ character, which is typified by a very low oscillator strength, the oscillator strength of the $1^2A''\rightarrow 4^2A''$ transition will therefore be reduced. In contrast, the $1^2A''\rightarrow 3^2A''$ transition should conserve the majority of its original oscillator strength. The outcome of these effects will be an inversion in the oscillator strengths of the $1^2A''\rightarrow 4^2A''$ and $1^2A''\rightarrow 3^2A''$ transitions relative to those of the static state cation radical.

Quantitative CASSCF calculations confirm the qualitative VBCM predictions. As shown in Table 5, the oscillator strength of the $1^2A''\rightarrow 4^2A''$ transition indeed decreases upon rotation of the phenyl group from the minimum energy, bisected geometry. As predicted from the VBCM model, the oscillator strength of the $1^2A''\rightarrow 3^2A''$ transition is affected to a much smaller extent; it increases slightly. Finally, the oscillator strength of the UV transition ($1^2A''\rightarrow 5^2A''$) remains unchanged. This is why the oscillator strength for this transition is normalized to the experimental peak intensity in Figure 3.

The changes in the oscillator strengths upon phenyl group rotation lead to better agreement between the calculated and experimental electronic spectra for $\mathbf{1}^{+\bullet}$. This is graphically illustrated in Figure 3, where the relative transition energies and oscillator strengths of the bisected cation radical (0°, unfilled bars) are compared to the cation radical with a phenyl twist angle of 30° (filled bars). Since the energy of this twisted structure is calculated to be only 1 kcal/mol higher than the bisected structure, it seems likely that the electronic spectrum of $\mathbf{1}^{+\bullet}$ will be averaged over a broad range of angles. Although, a more rigorous treatment might have been valuable, the current results already suggest that dynamical averaging is indeed required to properly account for the experimental spectrum of $\mathbf{1}^{+\bullet}$.

D. Summary

The structures of phenylcyclopropane ($\mathbf{1}^{+\bullet}$) and cumene ($\mathbf{2}^{+\bullet}$) cation radicals were calculated using CASSCF and B3LYP computational methods. Both methods predict that $\mathbf{1}^{+\bullet}$ adopts a delocalized, bisected structure. In contrast to $\mathbf{1}^{+\bullet}$, the spin and charge in $\mathbf{2}^{+\bullet}$ is largely localized in the phenyl ring. The CASPT2 method was used to predict the electronic spectra of $\mathbf{1}^{+\bullet}$ and $\mathbf{2}^{+\bullet}$. The large differences in the spectra of $\mathbf{1}^{+\bullet}$ and $\mathbf{2}^{+\bullet}$ can be traced to a larger degree of $\sigma-\pi$ interaction in $\mathbf{1}^{+\bullet}$. The results can be understood in terms of a simple valence bond configuration mixing model.

In general, the calculated transition energies were in good accord with the experimental values, however, the relative UV−vis peak intensities for $\mathbf{1}^{+\bullet}$ were not well reproduced if a static structure is assumed. Better agreement was obtained by considering the effect of vibrational averaging due to phenyl group rotation in $\mathbf{1}^{+\bullet}$. It will be interesting to see if similar behavior is observed for the electronic spectra of other cation radicals where conjugation between moieties can be affected by a low energy structural distortion.

Acknowledgment. Research support at Rochester was provided by the National Science Foundation (Grant CHE-9312460), at the Hebrew University was provided by the Israel Science Foundation and the Volkswagen Stiftung, at the Universitat de València by the Spanish DGICYT (PB94-0986), and at the Chemical Centre by the Swedish Natural Science Research Council (NFR) and by the European Commission through the TMR programme (Grant ERB FMRX-CT96-0079). We thank Professor Thomas Bally (University of Fribourg) for obtaining the matrix UV−vis spectrum of phenylcyclopropane cation radical.

References and Notes

(1) (a) Rao, V. R.; Hixson, S. S. *J. Am. Chem. Soc.* **1979**, *101*, 6458. (b) Mizuno, K.; Ogawa, J.; Otsuji, Y. *Chem. Lett.* **1981**, 741. (c) Roth, H. D.; Schilling, M. L. M. *J. Am. Chem. Soc.* **1981**, *103*, 7210. (d) Roth, H. D.; Schilling, M. L. M.; Hutton, R. S.; Truesdale, E. A. *J. Am. Chem. Soc.* **1983**, *105*, 153. (e) Mizuno, K.; Kamiyama, N.; Ichinose, N.; Otsuji, Y. *Tetrahedron* **1985**, *41*, 2207. (f) Abelt, C. J.; Roth, H. D.; Schilling, M. L. M. *J. Am. Chem. Soc.* **1985**, *107*, 4148. (g) Roth, H. D.; Schilling, M. L. M.; Schilling, F. C. *J. Am. Chem. Soc.* **1985**, *107*, 4152. (h) Shim, S. C.; Song, J. S. *J. Org. Chem.* **1986**, *51*, 2817. (i) Mazzocchi, P. H.; Somich, C.; Edwards, M.; Morgan, T.; Ammon, H. L. *J. Am. Chem. Soc.* **1986**, *108*, 6828. (j) Mazzocchi, P. H.; Somich, C. *Tetrahedron Lett.* **1988**, 513. (k) Dinnocenzo, J. P.; Todd, W. P.; Simpson, T. R.; Gould, I. R. *J. Am. Chem. Soc.* **1990**, *112*, 2463. (l) Hixson, S. S.; Xing, Y. *Tetrahedron Lett.* **1991**, 173. (m) Mizuno, K.; Ichinose, N.; Otsuji, Y. *J. Org. Chem.* **1992**, *57*, 1855. (n) Roth, H. D. *Top. Curr. Chem.* **1992**, *163*, 131. (o) Dinnocenzo, J. P.; Lieberman, D. R.; Simpson, T. R. *J. Am. Chem. Soc.* **1993**, *115*, 366. (p) Takahashi, Y.; Endoh, F.; Ohaku, H.; Wakamatsu, K.; Miyashi, T. *J. Chem. Soc. Chem. Commun.* **1994**, 1127. (q) Roth, H. D. *Adv. Theor. Interesting Mol.* **1995**, *3*, 261. (r) Dinnocenzo, J. P.; Simpson, T. R.; Zuilhof, H.; Lieberman, D. R.; Todd, W. P. *J. Am. Chem. Soc.* **1997**, *119*, 987. (s) Dinnocenzo, J. P.; Simpson, T. R.; Zuilhof, H.; Lieberman, D. R. *J. Am. Chem. Soc.* **1997**, *119*, 994. (t) Takahashi, Y.; Ohaku, H.; Nishioka, N.; Ikeda, H.; Miyashi, T.; Gormin, D. A.; Hilinski, E. F. *J. Chem. Soc., Perkin Trans. 2* **1997**, 303. (u) Wang, Y.; Tanko, J. M. *J. Am. Chem. Soc.* **1997**, *119*, 8201.

(2) (a) Becke, A. D. *J. Chem. Phys.* **1993**, *98*, 5648. (b) Stephens, P. J.; Devlin, F. J.; Chabalowski, C. F.; Frisch, M. J. *J. Phys. Chem.* **1994**, *98*, 11623.

(3) Andersson, K.; Malmqvist, P.-Å.; Roos, B. O.; Sadlej, A. J.; Wolinski, K. *J. Phys. Chem.* **1990**, *94*, 5483.

(4) Roos, B. O.; Fülscher, M. P.; Malmqvist, P.-Å.; Merchán, M.; Serrano-Andrés, L. *Understanding Chem. React.* **1995**, *13*, 357.

(5) (a) Roos, B. O.; Andersson, K.; Fülscher, M. P.; Malmqvist, P.-Å.; Serrano-Andrés, L.; Pierloot, K.; Merchán, M. In *Advances in Chemical Physics: New Methods in Computational Quantum Mechanics*; Prigogine, I., Rice, S. A., Eds.; Wiley: New York, 1996; Vol. XCIII, p 219. (b) Roos, B. O.; Merchán, M.; McDiarmid, R.; Xing, X. *J. Am. Chem. Soc.* **1994**, *116*, 5927.

(6) (a) Fülscher, M. P.; Matzinger, S.; Bally, T. *Chem. Phys. Lett.* **1995**, *236*, 167. (b) Rubio, M.; Merchán, M.; Ortí, E.; Roos, B. O. *J. Phys. Chem.* **1995**, *99*, 14980.

(7) (a) Shaik, S. S. In *New Theoretical Concepts for Understanding Organic Reactions*; NATO ASI Series C267; Bertram, J., Csizmadia, I. G., Eds., Kluwer Publications: Dordrecht, 1989. (b) Shaik, S.; Hiberty, P. C. *Adv. Quantum Chem.* **1995**, *26*, 99. (c) Pross, A. *Theoretical and Physical Principles of Organic Reactivity*; Wiley: New York, 1995.

(8) Eberson, L.; González-Luque, R.; Merchán, M.; Radner, F.; Roos, B. O.; Shaik, S. *J. Chem. Soc., Perkin Trans. 2* **1997**, 463.

(9) Frisch, M. J.; Trucks, G. W.; Schlegel, H. B.; Gill, P. M. W.; Johnson, B. G.; Robb, M. A.; Cheeseman, J. R.; Keith, T.; Petersson, G. A.; Montgomery, J. A.; Raghavachari, K.; Al-Laham, M. A.; Zakrzewski, V. G.; Ortiz, J. V.; Foresman, J. B.; Cioslowski, J.; Stefanov, B. B.; Nanayakkara, A.; Challacombe, M.; Peng, C. Y.; Ayala, P. Y.; Chen, W.; Wong, M. W.; Andres, J. L.; Replogle, E. S.; Gomperts, R.; Martin, R. L.; Fox, D. J.; Binkley, J. S.; Defrees, D. J.; Baker, J.; Stewart, J. P.; Head-Gordon, M.; Gonzalez, C.; Pople, J. A. *Gaussian 94*, Revision D.1; Gaussian, Inc.: Pittsburgh, PA, 1995.

(10) (a) Eriksson, L. A.; Malkin, V. G.; Malkina, O. L.; Salahub, D. R. *J. Chem. Phys.* **1993**, *99*, 9756. (b) Eriksson, L. A.; Malkin, V. G.; Malkina, O. L.; Salahub, D. R. *Int. J. Quantum Chem.* **1994**, *52*, 879. (c) Barone, V.; Adamo, C. *Chem. Phys. Lett.* **1994**, *224*, 432. (d) Huang, M. B.; Suter, H. U.; Engels, B.; Peyerimhoff, S. D.; Lunell, S. *J. Phys. Chem.* **1995**, *99*, 9724. (e) Shephard, M. J.; Paddon-Row, M. N. *J. Phys. Chem.* **1995**, *99*, 3101. (f) Zuilhof, H.; Dinnocenzo, J. P.; Reddy, C.; Shaik, S. *J. Phys. Chem.* **1996**, *100*, 15774.

(11) Andersson, K.; Fülscher, M. P.; Karlström, G.; Lindh, R.; Malmqvist, P.-Å.; Olsen, J.; Roos, B. O.; Sadlej, A. J.; Blomberg, M. R. A.; Siegbahn, P. E. M.; Kellö, V.; Noga, J.; Urban, M.; Widmark, P.-O. *MOLCAS Version 3*; Department of Theoretical Chemistry, Chemistry Center: University of Lund, P.O. Box 124, S-221 00 Lund, Sweden, 1994.

(12) Widmark, P.-O.; Malmqvist, P.-Å.; Roos, B. O. *Theor. Chim. Acta* **1990**, *77*, 291.

(13) (a) Hudson, C. E.; Giam, C. S.; McAdoo, D. J. *J. Org. Chem.* **1993**, *58*, 2017. (b) Krogh-Jespersen, K.; Roth, H. D. *J. Am. Chem. Soc.* **1992**, *114*, 8388 and references therein.

(14) Bruckmann, P.; Klessinger, M. *Chem. Ber.* **1974**, *107*, 1108.

(15) Kabakoff, D. S.; Namanworth, E. *J. Am. Chem. Soc.* **1970**, *92*, 3234.

(16) (a) Rao, D. N. R.; Chandra, R.; Symons, M. C. R. *J. Chem. Soc., Perkin Trans. 2* **1984**, 1201. (b) Kira, M.; Nakazawa, H.; Sakurai, H. *Chem. Lett.* **1985**, 1841.

(17) Kelsall, B. J.; Andrews, L. *J. Phys. Chem.* **1984**, *88*, 5893.

(18) (a) Dymerski, P. P.; Fu, E.; Dunbar, R. C. *J. Am. Chem. Soc.* **1974**, *96*, 4109. (b) Sehested, K.; Holcman, J.; Hart, E. J. *J. Phys. Chem.* **1977**, *81*, 1363. (c) Teng, H. H.-L.; Dunbar, R. C. *J. Chem. Phys.* **1978**, *68*, 3133. (d) Andrews, L.; Miller, J. H.; Keelan, B. W. *Chem. Phys. Lett.* **1980**, *71*, 207. (e) Miller, J. H.; Andrews, L.; Lund, P. A.; Schatz, P. N. *J. Chem. Phys.* **1980**, *73*, 4932. (f) Kim, E. K.; Bockman, T. M.; Kochi, J. K. *J. Am. Chem. Soc.* **1993**, *115*, 3091. (g) Yagci, Y.; Schnabel, W.; Wilpert, A.; Bendig, J. *J. Chem. Soc., Faraday Trans.* **1994**, *90*, 287.

(19) Bally, T. In *Radical Ionic Systems, Properties of Condensed Phase*; Lund, A., Shiotani, M., Eds.; Kluwer Academic Publishers: Dordrecht, 1991.

(20) Bally, T.; Nitsche, S.; Roth, K.; Haselbach, E. *J. Am. Chem. Soc.* **1984**, *106*, 3927.

(21) Kimura, K.; Katsumata, S.; Achiba, Y.; Yamazaki, T.; Iwata, S. *Handbook of HeI Photoelectron Spectra of Fundamental Organic Molecules*; Halsted: New York, 1981.

(22) Libit, L.; Hoffmann, R. *J. Am. Chem. Soc.* **1974**, *96*, 1370.